Mon. Not. R. Astron. Soc. **351,** 667–675 (2004) doi:10.1111/j.1365-2966.2004.07814.x

A comprehensive CCD photometric study of the open cluster NGC 2421

R. K. S. Yadav[1]★ and Ram Sagar[2,3]★

[1]*Inter-University Centre for Astronomy and Astrophysics, Ganeshkhind, Pune 411 007, India*
[2]*State Observatory, Manora Peak Nainital 263 129, India*
[3]*Aryabhatta Research Institute of Observational Sciences, Manora Peak Nainital 263 129, India*

Accepted 2004 March 5. Received 2004 March 3; in original form 2004 February 16

ABSTRACT

We present the *UBVRI* CCD photometry in the region of the open cluster NGC 2421. The radius of the cluster is determined as ∼3.0 arcmin using a stellar density profile. Our study indicates that the metallicity of the cluster is $Z \sim 0.004$. The reddening $E(B-V) = 0.42 \pm 0.05$ mag is determined using a two colour $(U-B)$ versus $(B-V)$ diagram. By combining the 2MASS *JHK* data with the optical data, we determined that $E(J-K) = 0.20 \pm 0.20$ mag and $E(V-K) = 1.15 \pm 0.20$ mag for this cluster. Colour-excess diagrams show a normal interstellar extinction law in the direction of the cluster. We determined that the distance of the cluster is 2.2 ± 0.2 kpc by comparing the zero-age main sequence with the intrinsic colour–magnitude diagram of the cluster. The age of the cluster has been estimated as 80 ± 20 Myr using the stellar isochrones of metallicity $Z = 0.004$. The mass function slope $x = 1.2 \pm 0.3$ has been derived by applying the corrections of field star contamination and data incompleteness. Our analyses indicate that the cluster NGC 2421 is dynamically relaxed.

Key words: Hertzsprung–Russell (HR) diagram – stars: luminosity function, mass function – dust, extinction – galaxies: clusters: individual: NGC 2421.

1 INTRODUCTION

The investigation of young open star clusters provides us with a powerful tool for understanding the structure and history of star formation in our Galaxy. In order to fully exploit the information provided by open clusters we must accurately know their ages, distances, reddenings, metal abundances and stellar contents. For this, multicolour CCD photometric observations have proved to be very useful. With the development of more accurate stellar models it has been possible to provide a better estimate of the cluster ages simply by comparing theoretical isochrones with the observed CCD colour–magnitude (CM) diagrams. So, In this paper we have considered the open cluster NGC 2421 with the aim of presenting new accurate CCD photometry. From this photometry we select photometric members and derive several fundamental parameters, such as distance, interstellar reddening, metallicity and age as well as luminosity (LF) and mass function (MF).

The young open cluster NGC 2421 = C0734−205 (α_{2000} = $07^{\rm h}36^{\rm m}16^{\rm s}$, $\delta_{2000} = -20^\circ 36' 44''$; $l = 236\overset{\circ}{.}24$, $b = 0\overset{\circ}{.}08$) is classified as a Trumpler class I2 m by Ruprecht (1966). This cluster was first studied by Moffat & Vogt (1975) photoelectrically and derived a distance of approximately 1.87 kpc, having $E(B-V) = 0.47 \pm 0.05$ mag and age less than 10^7 yr. Ramsay & Pollacco (1992) also studied this cluster using CCD photometry and found a colour excess $E(B-V) = 0.49 \pm 0.03$ mag but a distance of 2.75 kpc. To our knowledge no other studies have been carried out for the cluster NGC 2421 so far.

The layout of the paper is as follows. In Section 2 we briefly describe the observations, data reduction strategies and present a comparison with the previous photometry. Section 3 is devoted to the detailed analysis of the present photometric data for the determination of the cluster parameters. Finally, Section 4 summarizes the main results of the paper.

2 OBSERVATIONS AND DATA REDUCTION

UBV $R_c I_c$ CCD photometry was performed for the cluster NGC 2421 on 2003 February 24, 25 at the State Observatory Naini Tal with the 104-cm telescope (f/13) and a 2K × 2K CCD (24-μm pixels). The scale was 0.36 arcsec pixel^{-1}, giving 12.6 arcmin on a side. The read-out noise for the system was 5.3 e$^-$, while the gain was 10 e$^-$ adu^{-1}. Table 1 lists the log of our CCD observations. To improve the signal-to-noise (S/N) ratio, observations were made in 2 × 2 pixel binning mode while two to three deep exposures were taken for accurate photometric measurements of faint stars. Many bias frames were taken during the observations for removing the bias level in the images. Flat-field exposures were made of the twilight sky in each filter. Fig. 1 shows the finding chart for the stars that were brighter than $V = 20$ mag in the cluster NGC 2421. We observed the standard area PG 1633+099 (Landolt 1992) several times during the night for the purpose of the determination of atmospheric extinction coefficients and for the photometric calibration of

★E-mail: rkant@iucaa.ernet.in (RKSY); sagar@upso.ernet.in (RS)

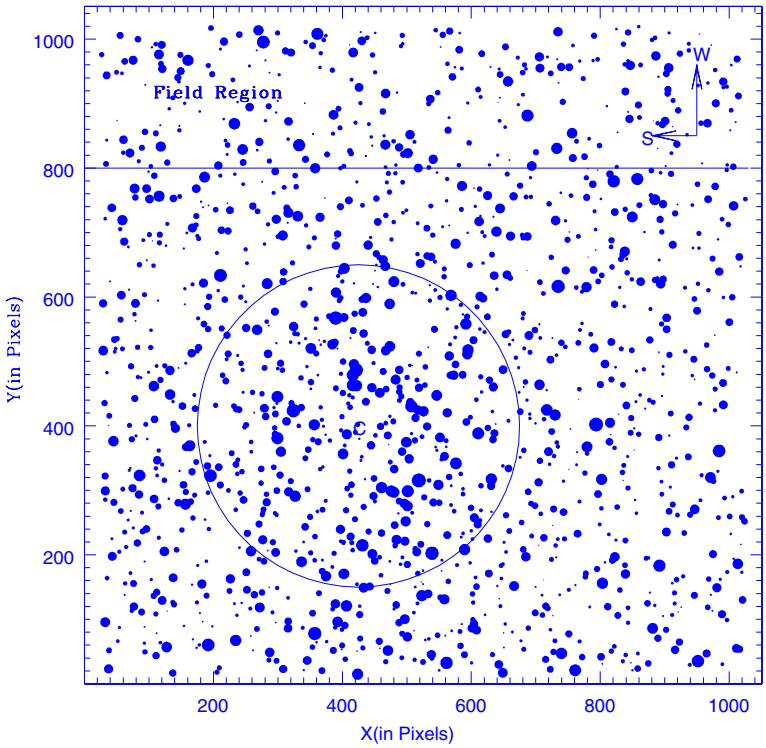

Figure 1. Finding chart of the stars in the cluster NGC 2421. The (X, Y) coordinates are in pixel units corresponding to 0.72 arcsec on the sky. Direction is indicated in the map. Filled circles of different sizes represent the brightness of the stars. Smallest size denotes stars of $V \sim 20$ mag. Open circles with a centre at 'C' in the chart represent the cluster size.

Table 1. Journal of observations, with dates and exposure times for each passband. N denotes the number of stars measured in different passbands.

Band	Exposure time (s)	Date	N
U	1800×2, 300×2	2003 Feb 24, 25	770
B	1200×2, 240×2	–	1200
V	900×3, 180×2	–	1300
R	500×3, 120×2	–	1350
I	300×3, 60×2	–	1400

the CCD system. The brightness and colour ranges of the standard stars are $13 \leqslant V \leqslant 15$ and $-0.2 \leqslant (V - I) \leqslant 1.1$, respectively. So, the standard stars in this area provide a good magnitude and colour range, essential for obtaining reliable photometric transformation.

The data were reduced using the computing facilities available at the Inter-University Centre for Astronomy and Astrophysics (IUCAA), Pune, India. Corrections to the raw data for bias and flat-fielding were performed using standard IRAF routines. The CCD frames of the same exposure for a given filter were combined to improve the statistics of the faintest stars. Stellar magnitudes were obtained by using the DAOPHOT software (Stetson 1987, 1992) and the conversion of the raw instrumental magnitudes into those of a standard photometric system were performed using procedures outlined by Stetson (1992). The instrumental magnitudes were derived through point spread function (PSF) fitting using DAOPHOT. To determine the PSF, we used several well isolated stars for the entire frame. Several stars brighter than $V = 11.0$ mag could not be measured as they saturated even on the shortest frame.

For translating the instrumental magnitude to the standard magnitude, the calibration equations derived using least-squares linear regression are as follows:

$$u = U + 4.95 \pm 0.01 - (0.02 \pm 0.01)(U - B) + 0.62X$$
$$b = B + 3.41 \pm 0.01 - (0.05 \pm 0.01)(B - V) + 0.28X$$
$$v = V + 3.05 \pm 0.01 - (0.09 \pm 0.01)(B - V) + 0.17X$$
$$r = R + 2.96 \pm 0.01 - (0.02 \pm 0.01)(V - R) + 0.12X$$
$$i = I + 3.29 \pm 0.01 - (0.07 \pm 0.01)(R - I) + 0.10X,$$

where U, B, V, R and I are the standard magnitudes and u, b, v, r and i are the instrumental aperture magnitudes normalized for 1 s of exposure time and X is the airmass. We have ignored the second-order colour correction terms as they are generally small in comparison to other errors present in the photometric data reduction. The errors in zero points and colour coefficients are $\sim$0.01 mag. The errors in magnitude and colour are plotted against V magnitude in Fig. 2 and the mean values of the errors are listed in Table 2. The final photometric data are available in electronic form at the WEBDA site[1] and also from the authors.

2.1 Comparison with previous photometry

We have obtained *UBVRI* photometry for $\sim$1300 stars down to $V = 20$ mag in the region of NGC 2421. Ramsay & Pollacco (1992) have also presented CCD *UBV* photometry for 98 stars. Fig. 3 shows the plots of difference Δ in V, $(B - V)$ and $(U - B)$ with V magnitude. The average difference (in the sense: our values minus Ramsay & Pollacco 1992) along with their standard deviation are listed in

[1] http://obswww.unige.ch/webda/

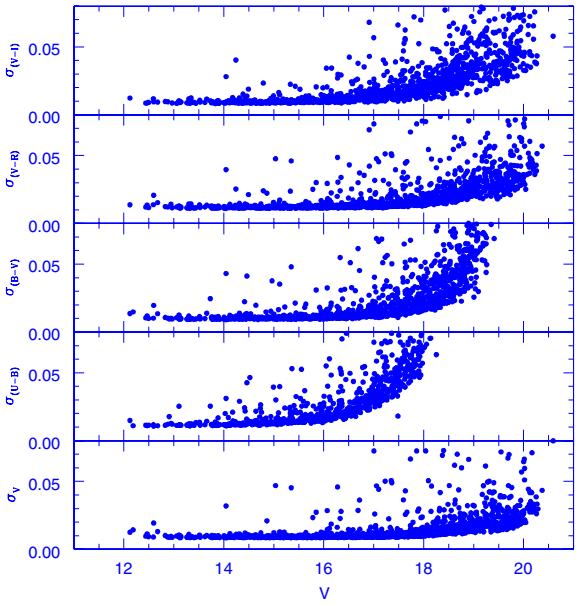

Figure 2. Photometric errors in magnitude and colour against V magnitude.

Table 2. Mean photometric errors in magnitude and colours in different magnitude bins.

V	σ_V	σ_{U-B}	σ_{B-V}	σ_{V-R}	σ_{V-I}
12–13	0.014	0.012	0.014	0.011	0.010
13–14	0.010	0.012	0.011	0.012	0.009
14–15	0.010	0.014	0.011	0.012	0.010
15–16	0.010	0.017	0.011	0.012	0.011
16–17	0.010	0.025	0.013	0.013	0.014
17–18	0.011	0.038	0.017	0.016	0.015
18–19	0.019		0.018	0.025	0.035
19–20	0.023		0.025	0.035	0.054

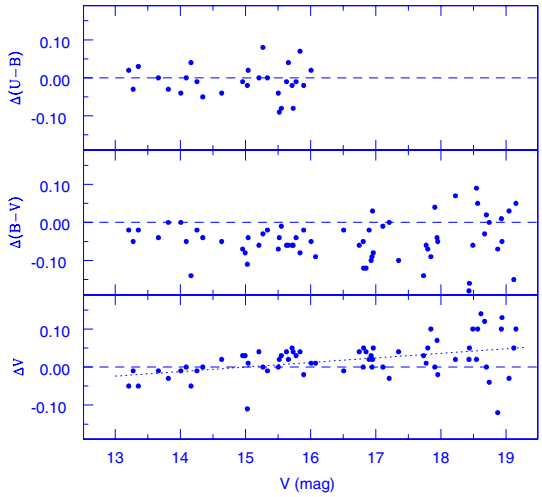

Figure 3. Comparison of our *UBV* photometry with the CCD photometry given by Ramsay & Pollacco (1992). The dotted line represents a linear least-squares fitting to the data points.

Table 3. Comparison of the present CCD photometry with Ramsay & Pollacco (1992). The difference (Δ) is always in the sense of the present minus the comparison data. The mean along with their standard deviations in magnitude are based on N stars. The few deviated points are not included in the average determination.

V range	$\langle\Delta V\rangle$ Mean$\pm\sigma$(N)	$\langle\Delta(B-V)\rangle$ Mean$\pm\sigma$(N)	$\langle\Delta(U-B)\rangle$ Mean$\pm\sigma$(N)
13.0–14.0	$-0.02 \pm 0.02(5)$	$-0.02 \pm 0.02(5)$	$0.00 \pm 0.02(5)$
14.0–15.0	$0.00 \pm 0.02(8)$	$-0.04 \pm 0.02(8)$	$0.00 \pm 0.04(8)$
15.0–16.0	$0.02 \pm 0.02(14)$	$-0.04 \pm 0.02(14)$	$-0.01 \pm 0.05(15)$
16.0–17.0	$0.02 \pm 0.02(12)$	$-0.05 \pm 0.04(9)$	
17.0–18.0	$0.02 \pm 0.04(10)$	$-0.04 \pm 0.04(9)$	
18.0–19.0	$0.03 \pm 0.04(8)$	$-0.00 \pm 0.05(10)$	

Table 3. The comparison of our and their V magnitudes shows a weak linear dependence of ΔV with V, which is shown by the dotted line in Fig. 3. A systematic difference of ~ -0.03 mag is present in $(B-V)$ colour without any dependence on stellar magnitude, while there is no significant difference or dependence seen in $(U-B)$ colour with stellar magnitude.

3 DATA ANALYSIS

3.1 Cluster radius

We used a radial stellar density profile for the determination of cluster radius. For this, we selected the stars that were brighter than $V = 20.0$ mag. The average stellar density was calculated in successive, 50-pixel wide annuli around the cluster centre. The cluster centre is determined iteratively by calculating average the X and Y position of the stars within 400 pixels from an eye estimated centre, until they converged to a constant value. In this way, we obtained the pixel coordinate of the cluster centre as (425, 400), which is marked by 'C' in the Fig. 1. Fig. 4 shows the stellar surface density as a function of distance from the cluster centre. The density profile flattens at a radius of $r = 250$ pixels. After $r = 250$ pixels stellar density merges into the field star density as indicated by the horizontal arrow in Fig. 4. The surface density of the field stars is derived as 7 $\times 10^{-4}$ per pixel^2. In this way we estimated a radius of 3.0 arcmin for this cluster, which is smaller than the value of 3.5 arcmin given by Mermilliod (1995).

We observed a 12.5×12.5 arcmin^2 area towards the cluster NGC 2421, which is larger than the cluster radius and hence we have considered the stars as field stars that have a position of more than 1.6 cluster radius (see Fig. 1). The nearest boundary of the field region is approximately 5.0 arcmin away from the cluster centre in the west direction.

3.2 Apparent colour–magnitude diagrams of the cluster and field regions

In Fig. 5 we present photometric colour–magnitude diagrams of the cluster and field region. To reduce the field star contamination in the CM diagrams, we used the stars within the cluster radius. The CM diagrams of the cluster extend down to $V \sim 19.5$ mag except in the V, $(U-B)$ CM diagram where it is only up to $V \sim 18$ mag. A main-sequence extending up to $V = 19.0$ mag is clearly visible in the CM diagrams of the cluster. Contamination due to the field stars is evident, especially in the fainter parts of the CM diagrams. Ideally, one would like to eliminate the contamination from the stars of the galactic field using the information contained in the proper motion or the radial velocity of the stars. Unfortunately, these studies

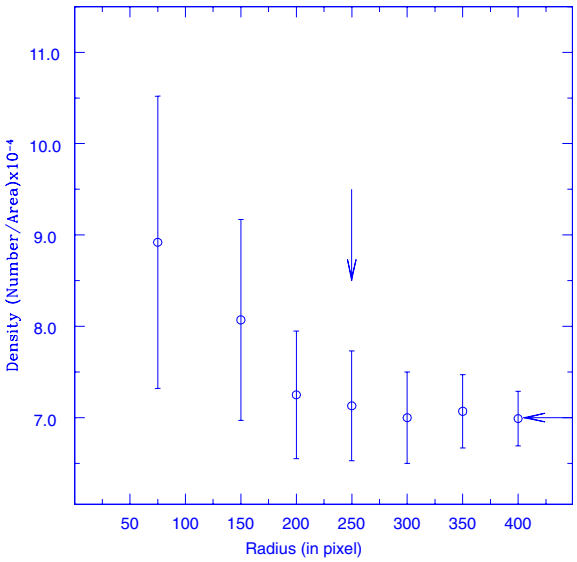

Figure 4. Star density as a function of radial distance from the centre of the cluster with stars brighter than $V = 20.0$ mag. Errorbars denote the error determined from sampling statistics ($=1/\sqrt{N}$, where N is the number of stars used in the density estimation at that point). Horizontal and vertical arrows represent the density of the field stars and the radius of the cluster, respectively.

are not available for this cluster and hence we are forced to base our analysis on photometric arguments. We selected members by defining the binary sequence, this was defined by shifting the blue envelope by 0.80 mag vertically, which is shown in the CM diagram of the cluster. In Table 4, we have listed the expected number of field stars using the $V, (V - I)$ CM diagram of the field region. From this table we can estimate the frequency distribution of stars in different parts of the CM diagram. It is also clear that all photometric probable members cannot be cluster members and non-members should be

Table 4. Frequency distribution of the stars in the $V, (V - I)$ diagram of the cluster and field regions. N_B, N_S and N_R denote the number of stars in a magnitude bin blueward, along and redward of the cluster sequence, respectively. The number of stars in the field regions are corrected for area differences. N_C (difference between the N_S value of cluster and field regions) denotes the statistically expected number of cluster members in the corresponding magnitude bin.

V range	Cluster region			Field region			
	N_B	N_S	N_R	N_B	N_S	N_R	N_C
12–13	0	4	2	0	0	3	4
13–14	0	13	7	0	0	6	13
14–15	0	26	10	0	8	10	18
15–16	0	38	14	0	10	19	28
16–17	1	52	10	0	22	15	30
17–18	21	57	11	0	24	24	33
18–19	24	47	11	1	37	35	10

subtracted in the studies of cluster mass functions etc. However, probable members located within a cluster radius from its centre can be used to determine the cluster parameters, as they have relatively less field star contamination and this has been done in the following sections.

3.3 Colour–colour diagram

We present a colour–colour (CC) diagram in Fig. 6. The zero-age main sequence (ZAMS) given by Schmidt-Kaler (1982) is shown by the continuous curve. It is clearly seen that this ZAMS does not fit for the stars of A and F spectral type. Prominent excess in the $(U - B)$ colour is clearly visible for the stars of $(B - V) > 0.50$ mag. This indicates that the cluster is metal deficient. The ultraviolet excess $\delta(U - B)$ determined with respect to Hyades MS turns out to be $\sim$0.15 mag. We estimated [Fe/H]~ -0.45 ($Z \sim 0.004$) adopting the [Fe/H] versus $\delta(U - B)$ relation by Carney (1979). Furthermore,

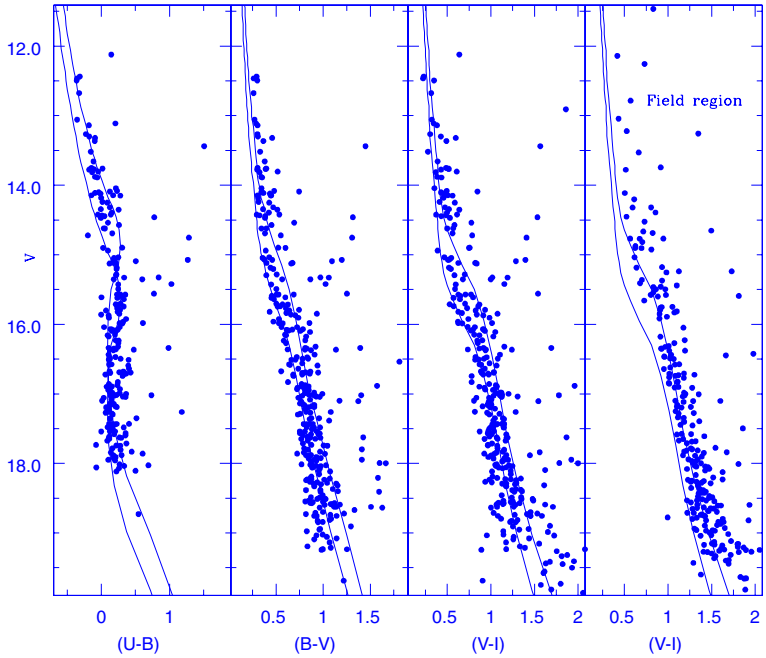

Figure 5. The $V, (U - B)$; $V, (B - V)$ V and $V, (V - I)$ CM diagrams for the stars within the cluster radius and the $V, (V - I)$ CM diagram for the field region. Solid lines represent the blue and red envelopes of the cluster MS. The red envelope is determined by shifting the blue envelope vertically by 0.80 mag.

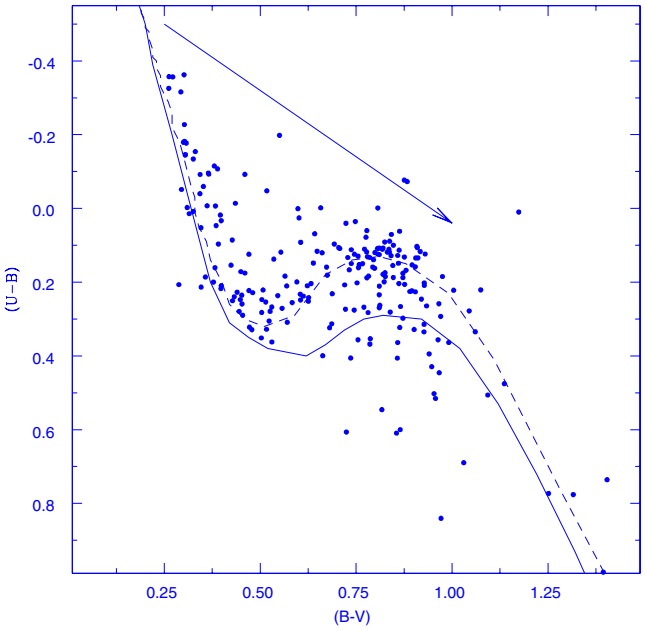

Figure 6. The $(U-B)$ versus $(B-V)$ colour–colour diagram of the cluster. The continuous straight line represents a slope of 0.72 and the direction of reddening vector, while the continuous curve represents locus of Schmidt-Kaler's (1982) ZAMS for solar metallicity. The curve shown by short dashed lines is the ZAMS given by Bertelli et al. (1994) for $Z = 0.004$.

Table 5. A comparison of the colour excess ratios with $E(B-V)$ with the normal interstellar extinction law given by Cardelli et al. (1989).

Object	$\frac{E(U-B)}{E(B-V)}$	$\frac{E(V-R)}{E(B-V)}$	$\frac{E(V-I)}{E(B-V)}$
Normal interstellar	0.72	0.65	1.25
NGC 2421	0.73 ± 0.06	0.54 ± 0.08	1.25 ± 0.11

we fitted the ZAMS given by Bertelli et al. (1994) for $Z = 0.004$ to determine the reddening in the direction of the cluster. The ZAMS of $Z = 0.004$, which is shown by short dash lines in the two colour diagram fits well and provides the reddening $E(B-V) = 0.42 \pm 0.05$ for this cluster. Our reddening estimate is in agreement with the earlier findings (see Section 1).

The nature of the extinction law has also been studied by using the stars that have a spectral type earlier than A0. We selected these stars using CC and CM diagrams and found that the stars with $V \leqslant 15.0$ mag and $(B-V) \leqslant 0.50$ mag are the desired stars. In the absence of spectral class information, we determined their intrinsic colour using the *UBV* photometric Q-method (cf. Johnson & Morgan 1953) and the calibrations provided by Caldwell et al. (1993) for $(U-B)_0$, $(V-R)_0$ and $(V-I)_0$ with $(B-V)_0$. Table 5 lists the mean values of the colour excess ratios. These values indicate that law of interstellar extinction is normal in the direction of the cluster.

3.4 Interstellar extinction in near-infrared

Two Micron All-sky Survey (2MASS) JHK_s data are available for 180 stars in this cluster and have been used for determining the interstellar extinction in the direction of the cluster in near-infrared (IR). The data are complete up to 16.0 mag in J, 15.5 mag in H and 15.0 mag in K_s. The K_s magnitudes are converted into K magnitudes following Persson et al. (1998). By combining optical and near-IR

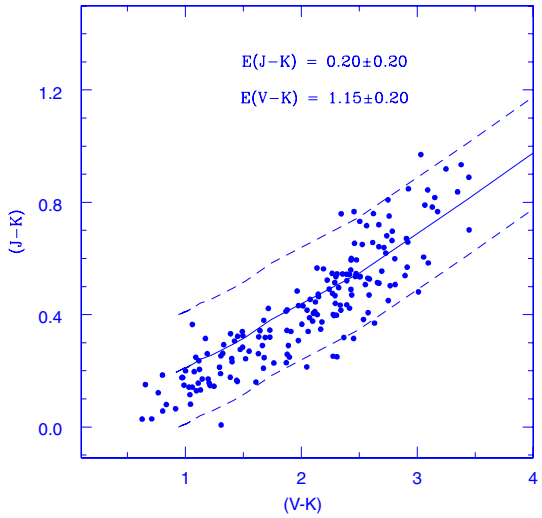

Figure 7. The plot of $(J-K)$ versus $(V-K)$ colour–colour diagram of the cluster for the stars within the cluster radius. The solid line is the ZAMS of $Z = 0.004$ fitted for the marked values of the excesses while the short dash lines show the errorbars.

data, we plotted a $(J-K)$ versus $(V-K)$ diagram in Fig. 7. The ZAMS shown by the solid line is taken from Bertelli et al. (1994) for $Z = 0.004$. The fit of ZAMS provides $E(J-K) = 0.20 \pm 0.20$ mag and $E(V-K) = 1.15 \pm 0.20$ mag for the cluster. The ratio $\frac{E(J-K)}{E(V-K)} \sim 0.18 \pm 0.30$ is in good agreement with the normal interstellar extinction value 0.19 suggested by Cardelli, Clayton & Mathis (1989).

3.5 Colour excess diagram

In Fig. 8, we plotted a colour-excess diagram for the study of the interstellar extinction law using optical and near-IR data. Colour excesses have been determined by comparing the observed colours of stars earlier than the A0 spectral type (see Section 3.3) with its intrinsic colours derived from the colour relation given by FitzGerald (1970) for $(U-B)$ and $(B-V)$; Johnson & Morgan (1966) for $(V-R)$ $(V-I)$ and Koornneef (1983) for $(V-J)$, $(V-H)$ and $(V-K)$. The colour excesses $E(U-B)$, $E(B-V)$, $E(V-R)$, $E(V-I)$, $E(V-H)$, and $E(V-K)$ are plotted against $E(V-J)$ in Fig. 8. The solid straight line shown in this figure is the least-squares linear fit to the data point. In all the colour-excess diagrams except $E(U-B)$ versus $E(V-J)$ and $E(B-V)$ versus $E(V-J)$, the values of the correlation coefficient (r) and the fit indicate that the data points are well represented by the linear relation. In $E(U-B)$ versus $E(V-J)$ and $E(B-V)$ versus $E(V-J)$ colour excess diagrams, scattering is more pronounced in the colour excess $E(U-B)$ and $E(B-V)$. In Table 6, we have listed the slope of the straight lines that represent the reddening directions in the form of colour excess ratios. The colour excess ratios given by Cardelli et al. (1989) for normal interstellar matter are also listed in this table. The present reddening directions generally agree within 3σ with those given for the normal interstellar extinction law. This indicates that the interstellar extinction law is normal in the direction of the cluster.

Furthermore, to understand the nature of interstellar extinction law in the direction of the cluster, we have determined the value of R. We used the relation $R = 1.1E(V-K)/E(B-V)$ given by Whittet & van Breda (1980), which is generally used for longer wavelengths. In this way we determined the value of $R = 3.2 \pm 0.3$,

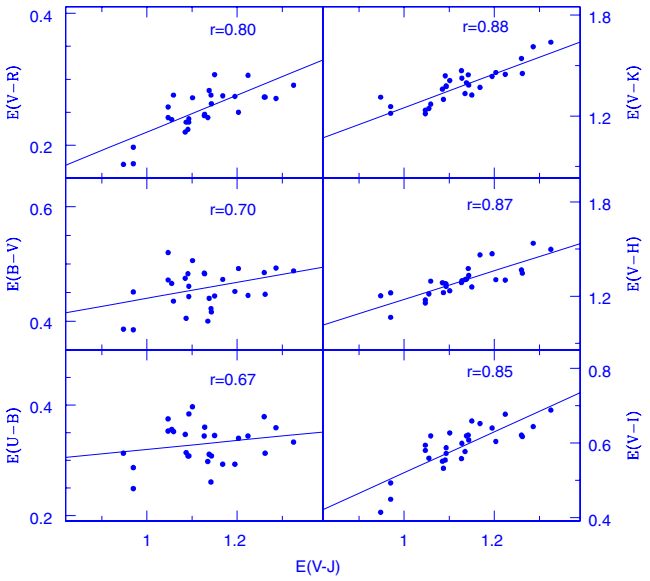

Figure 8. The plot of $E(U-B)$, $E(B-V)$, $E(V-R)$, $E(V-I)$, $E(V-H)$, $E(V-K)$ versus $E(B-V)$, colour excess diagram of the cluster. The solid straight lines represent the least-squares linear fit to the data point, while r denotes its correlation coefficients.

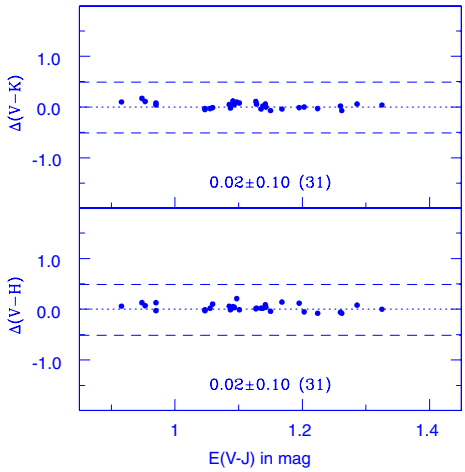

Figure 9. The plot of $\Delta(V-H)$ and $\Delta(V-K)$ versus $E(V-J)$. The horizontal dotted lines denote zero excess, while the short dashed lines denote the extent of the expected errors.

which is in agreement with the value of 3.1 for the normal extinction law.

On the basis of above analysis, we can conclude that interstellar extinction law is normal in the direction of the cluster and is in agreement with our earlier result.

3.6 Near-IR excess fluxes

To study the near-IR flux in the stars, we plot $\Delta(V-H)$ and $\Delta(V-K)$ versus $E(V-J)$ in Fig. 9. The value of $\Delta(V-H)$ and $\Delta(V-K)$ has been calculated by taking the difference between the observed colour excess in $(V-H)$ and $(V-K)$ based on spectral type and the derived colour excess from $E(V-J)$ assuming the normal interstellar extinction law. The possible source of errors may be the observational uncertainties in the *JHK* magnitudes, inaccuracies in the estimation of $E(V-J)$ and in its ratio with $E(V-H)$ and $E(V-K)$; and errors in the spectral and luminosity classifications. Consequently, the differences can be considered to be statistically significant only if their absolute values are larger than $\sim$0.5 mag. Fig. 9 gives an indication that for all the stars the values of $\Delta(V-H)$ and $\Delta(V-K)$ are close to zero. Hence, we can conclude that near-IR fluxes are not seen in any of the stars under study, indicating the absence of gas and dust envelopes around them.

3.7 Distance to the cluster

The distance of the cluster is determined by fitting the ZAMS. The intrinsic CM diagram of the cluster is depicted in Fig. 10. In order to reduce the field star contamination, we have only used the probable cluster members that are within the cluster radius and photometric members (see Section 3.2). For converting apparent V magnitude and $(U-B)$, $(B-V)$, $(V-R)$ and $(V-I)$ colours into the intrinsic one, we used average values of $E(B-V)$ and the following relations for $E(U-B)$ (cf. Kamp 1974), A_V and $E(V-I)$ (Walker 1987) and $E(V-R)$ (Alcalá & Ferro 1988)

$$E(U-B) = [X + 0.05E(B-V)]E(B-V),$$

where

$$X = 0.62 - 0.3(B-V)_0 \text{ for } (B-V)_0 < -0.09$$

and

$$X = 0.66 + 0.08(B-V)_0 \text{ for } (B-V)_0 > -0.09$$

$$A_V = [3.06 + 0.25(B-V)_0 + 0.05E(B-V)]E(B-V);$$

and

$$E(V-R) = [E1 + E2E(B-V)]E(B-V),$$

where

$$E1 = 0.6316 + 0.0713(B-V)_0$$

and

$$E2 = 0.0362 + 0.0078(B-V)_0;$$

$$E(V-I) = 1.25[1 + 0.06(B-V)_0 + 0.014E(B-V)]E(B-V).$$

The ZAMS taken from Bertelli et al. (1994) for $Z = 0.004$ is plotted in V_0, $(U-B)_0$; V_0, $(B-V)_0$; V_0, $(V-R)_0$ and V_0, $(V-I)_0$ diagrams. The visual fit of the ZAMS to the bluest envelope of the intrinsic CM diagrams provides $(m-M)_0 = 11.7 \pm 0.2$ mag for the cluster NGC 2421. The distance value of the cluster should be reliable since it has been derived by fitting the ZAMS over a wide range of MS. The distance modulus determined above gives a distance of 2.2 ± 0.2 kpc for the cluster. Our derived value of

Table 6. A comparison of the extinction law in the direction of the cluster with a normal extinction law given by Cardelli et al. (1989).

Objects	$\frac{E(U-B)}{E(V-J)}$	$\frac{E(B-V)}{E(V-J)}$	$\frac{E(V-R)}{E(V-J)}$	$\frac{E(V-I)}{E(V-J)}$	$\frac{E(V-H)}{E(V-J)}$	$\frac{E(V-K)}{E(V-J)}$	$\frac{E(J-K)}{E(V-K)}$
Normal value	0.32	0.43	0.27	0.56	1.13	1.21	0.19
NGC 2421	0.10 ± 0.09	0.14 ± 0.10	0.28 ± 0.05	0.55 ± 0.08	0.98 ± 0.13	1.08 ± 0.12	0.18 ± 0.30

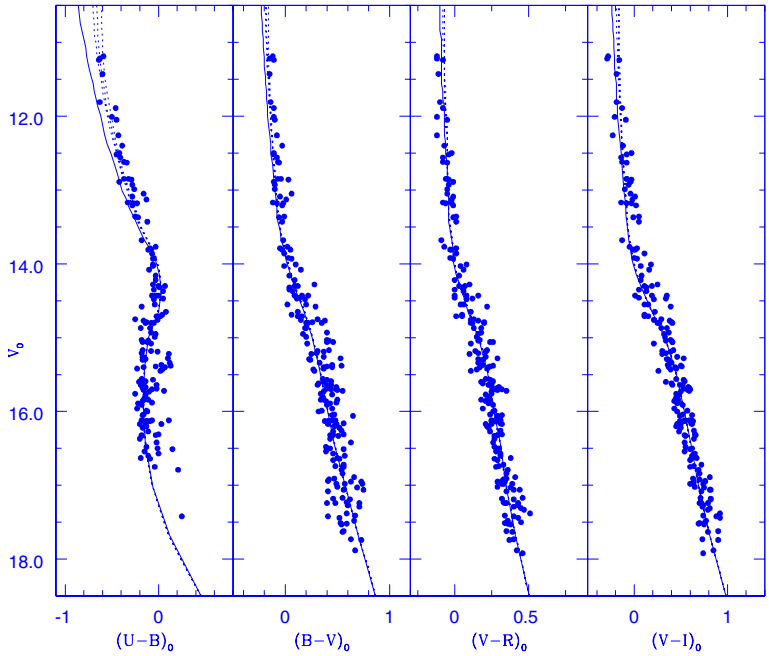

Figure 10. The intrinsic colour–magnitude diagram of the cluster. The solid curves are the ZAMS given by Bertelli et al. (1994) for $Z = 0.004$. The short dashed curves are the isochrones taken from Bertelli et al. (1994) for $Z = 0.004$ and log(age) = 7.8, 7.9 and 8.0.

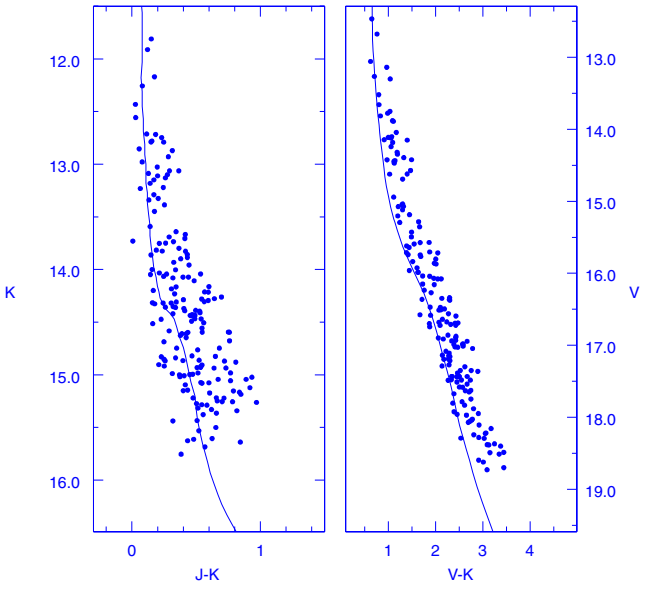

Figure 11. The K versus $(J - K)$ and V versus $(V - K)$ CM diagrams of the cluster using probable cluster members. The solid curve represents the isochrones of log(age) = 8.0 taken from Bertelli et al. (1994) for $Z = 0.004$.

the distance is not very different from the value of 1.9 kpc derived by Moffat & Vogt (1975), while it is less than the value of 2.8 kpc derived by Ramsay & Pollacco (1992).

3.8 Age of the cluster

The age of the cluster is determined by comparing the theoretical stellar evolutionary isochrones given by Bertelli et al. (1994) for $Z = 0.004$ with its intrinsic CM diagram (Fig. 10). The isochrones include the effect of mass loss and convective core overshooting in the model. We have fitted the isochrones of log(age) = 7.8, 7.9 and 8.0 to the intrinsic CM diagrams. The isochrones fitted to the brighter stars indicate that age of the cluster is 80 ± 20 Myr.

To derive the age and distance of the cluster with the combination of optical and near-IR data, we plot a V versus $(V - K)$ and K versus $(J - K)$ CM diagram in Fig. 11. The theoretical isochrones given by Bertelli et al. (1994) for $Z = 0.004$ and log(age) = 8.0 have been overplotted in the CM diagram. The apparent distance moduli $(m - M)_{V,(V-K)}$ and $(m - M)_{K,(J-K)}$ turn out to be 13.0 ± 0.3 and 11.8 ± 0.3 mag for this cluster. Using the reddening values estimated in Section 3.4, we derived a distance of 2.3 ± 0.3. Both age and distance determination for the cluster are thus in agreement with our earlier estimates. However, scattering is larger, due to the large errors in *JHK* mag.

3.9 Luminosity and mass function

To determine the luminosity function of the cluster, we considered the V versus $(V - I)$ CM diagram in comparison with others because it is the deepest. To remove the field star contamination, we adopted the photometric criteria by defining the blue and red envelope for the MS (see Section 3.2). The same envelope is also drawn for the V versus $(V - I)$ CM diagram of the field region. Stars are counted within this envelope, for both the cluster and the field region CM diagrams. The observed cluster luminosity function is the difference between the counts in the two fields after accounting for the difference in area between the cluster and field regions.

Incompleteness corrections are handled by introducing a number of artificial stars into the original data images of the V and I passband. The method used for this has been described in Yadav & Sagar (2002), so we only present the results here. Table 7 shows the completeness factor (CF) in the cluster region. To summarize, the completeness in the cluster region for MS stars is found to be 93.0 per cent at $V = 19.0$ mag. The completeness in the field region has been considered to be 100 per cent.

Table 7. Variation of the completeness factor in the $V, (V-I)$ diagram with the MS brightness.

V mag range	CF
12–13	0.99
13–14	0.99
14–15	0.99
15–16	0.96
16–17	0.94
17–18	0.93
18–19	0.93

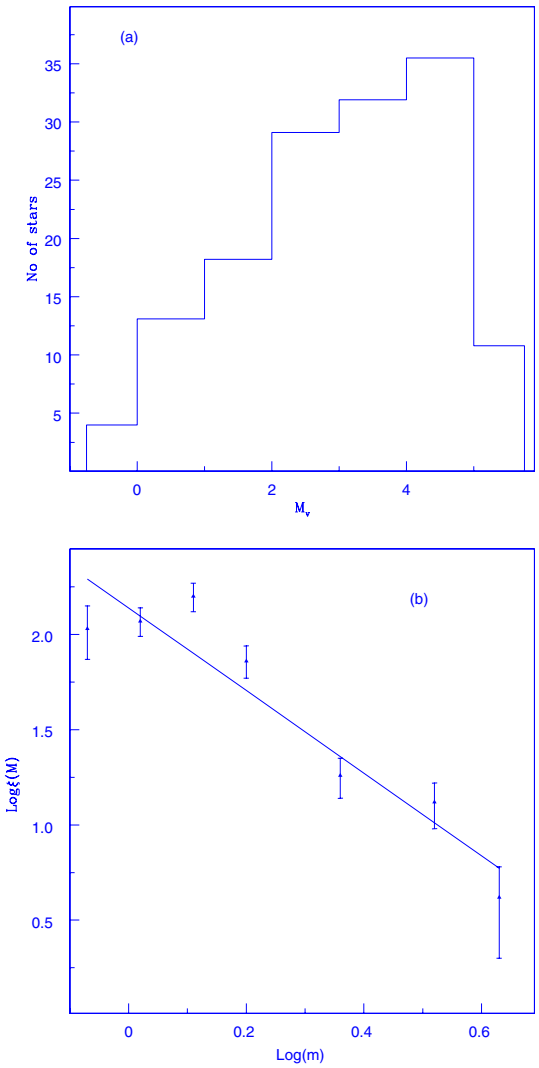

Figure 12. (a) Luminosity function of the cluster. (b) Mass function derived using Bertelli et al. (1994) isochrones.

The final corrected star counts are found by applying the incompleteness corrections in the cluster region. Fig. 12(a) shows the final luminosity function for the cluster NGC 2421. The luminosity function of the cluster rises until $M_v = 4.5$ and then decreases.

The mass function can be derived by using the relation $\log \frac{dN}{dM} = -(1+x)\log(M) + \text{constant}$, where d$N$ represents the number of stars in a mass bin dM with central M and x is the slope of the MF. In transferring the LF to the MF, we need theoretical evolutionary tracks and an accurate knowledge of the cluster parameters such as reddening, distance, age, etc. Theoretical models given by Bertelli et al. (1994) have been used to convert LF to MF and the resulting MF is shown in Fig. 12(b). The derived slope of the MF is $x = 1.2 \pm 0.3$ is in agreement, within the error, with the value of 1.35 given by Salpeter (1955) for the Solar neighbourhood stars.

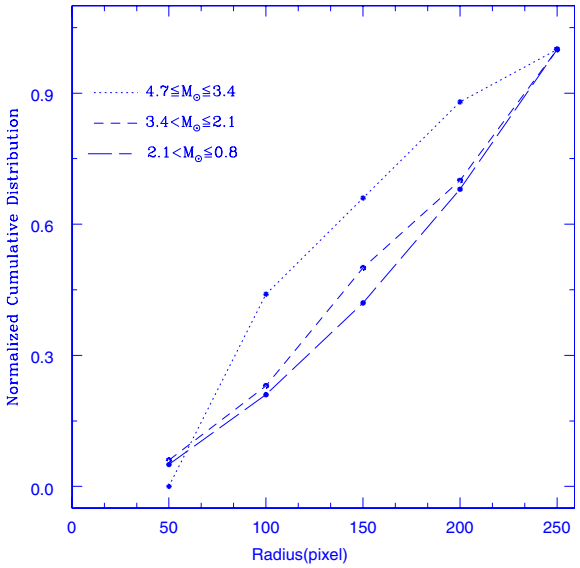

Figure 13. The cumulative radial distribution of stars in various mass ranges.

3.10 Dynamical state and mass segregation

In the lifetime of a star cluster encounters between its member stars gradually lead to an increased degree of energy equipartition throughout the cluster. The most significant consequence of this process is that the higher-mass cluster stars gradually sink towards the cluster centre and in the process transfer their kinetic energy to the more numerous lower-mass stellar components, thus leading to mass segregation. The time-scale in which a cluster will have lost all traces of its initial conditions is well represented by the relaxation time T_E. It is given by

$$T_E = \frac{8.9 \times 10^5 N^{1/2} R_{\rm h}^{3/2}}{\langle m \rangle^{1/2} \log(0.4N)},$$

where N is the number of cluster members, $R_{\rm h}$ is the half-mass radius of the cluster and $\langle m \rangle$ is the mean mass of the cluster stars (cf. Spitzer & Hart 1971). The value of $R_{\rm h}$ has been assumed to be half of the cluster radius derived by us. Using distance, the angular value of the radius has been converted into linear value. The probable cluster members are selected using the CM diagram of the cluster after removing the field star contamination and applying data incompleteness corrections. In this way, we estimated the dynamical relaxation time $T_E = 30$ Myr for this cluster, which implies that the cluster age is 2.6 times its relaxation age. Therefore, we can conclude that the cluster is dynamically relaxed.

To investigate the sign of mass segregation, we split the cluster members into three mass ranges $4.7 \leqslant M_\odot < 3.4$, $3.4 \leqslant M_\odot < 2.1$ and $2.1 \leqslant M_\odot \leqslant 0.8$. Fig. 13 shows the cumulative radial stellar distribution of stars for different masses. To examine the distribution of stars whether they belong to the same distribution or not, we performed a Kolmogorov–Smirnov (KS) test among these

distribution. The KS test provides the sign of mass segregation at a confidence level of 85 per cent. In the previous paragraph, we saw that this cluster is dynamically relaxed and hence one of the possible causes of mass segregation may be the dynamical evolution of the cluster.

4 CONCLUSIONS

We have investigated the area of the open cluster NGC 2421 using *UBVRI* CCD and 2MASS JHK_s data. The main results of our analysis are given below.

(i) The radius of the cluster is determined to be 3.0 arcmin, which corresponds to 1.9 pc at the distance of the cluster.

(ii) We estimated the abundance of the cluster stars as $Z = 0.004$ using excess in $(U - B)$. The $(U - B)$ versus $(B - V)$ colour–colour diagram yields $E(B - V) = 0.42 \pm 0.05$. The analysis of the *JHK* data in combination with the optical data provide $E(J - K) = 0.20 \pm 0.20$ mag and $E(V - K) = 1.15 \pm 0.20$ mag. Our analysis shows that the interstellar extinction law is normal towards the cluster direction. No stars were found that have near-IR fluxes due to the presence of circumstellar material around them.

(iii) A ZAMS fitting procedure gives a distance of 2.2 ± 0.2 kpc for this cluster, which is also supported by the value of 2.3 ± 0.3 kpc determined by us using the optical and near-IR data. An age of 80 ± 20 Myr is determined using the isochrones of $Z = 0.004$ given by Bertelli et al. (1994).

(iv) The mass function slope $x = 1.2 \pm 0.3$ is derived by considering the corrections of field star contamination and data incompleteness. Our analyses indicate that the cluster NGC 2421 is dynamically relaxed and one plausible reason for this relaxation may be the dynamical evolution of the cluster.

ACKNOWLEDGMENTS

We thank the referee for valuable comments, which have improved the quality of this paper. This study made use of 2MASS and WEBDA.

REFERENCES

Alcalá J.M., Ferro A.A., 1988, Rev. Mex. Astro. Astrofis, 16, 81
Bertelli G., Bressan A., Chiosi C., Fagotto F., Nasi E., 1994, A&AS, 106, 275
Caldwell A.R. John, Cousins A.W.J., Ahlers C.C., Wamelen P. van, Maritz E.J., 1993, SAAO Circ. No. 15
Cardelli J.A., Clayton G.C., Mathis J.S., 1989, ApJ, 345, 245
Carney B.W., 1979, ApJ, 233, 211
FitzGerald M.P., 1970, A&A, 4, 234
Johnson H.L., Morgan W.W., 1953, ApJ, 117, 313
Johnson H.L., Morgan W.W., 1966, ARA&A, 4, 193
Kamp L.W., 1974, A&AS, 16, 1
Koornneef J., 1983, A&A, 128, 84
Landolt A.U., 1992, AJ, 104, 340
Mermilliod J.C., 1995, in Egret E., Abrecht M.A., eds, Information and on-line data in Astronomy. Kulwer Academic Press, Dordrecht, p. 227
Moffat A.F.J., Vogt N., 1975, A&AS, 20, 85
Persson S.E., Murphy D.C., Krzeminski W., Roth M., Rieke M.J., 1998, AJ, 116, 2475
Ramsay G., Pollacco D.L., 1992, A&AS, 94, 73
Ruprecht J., 1966, Bull. Astron. Inst. Czech., 17, 33
Salpeter E.E., 1955, ApJ, 121, 161
Schmidt-Kaler Th., 1982, in Scaifers K., Voigt H.H., eds, Landolt/Bornstein, Numerical Data and Functional Relationship in Science and Technology, New series, Group VI, Vol. 2b. Springer-Verlag, Berlin, p. 14
Spitzer L., Hart M.H., 1971, ApJ, 164, 399
Stetson P.B., 1987, PASP, 99, 191
Stetson P.B., 1992, in Warrall D.M., Biemesderfer C., Barnes J. eds, ASP Conf. Ser. Vol. 25, Astronomical Data Analysis Software and System I. Astron. Soc. Pac., San Francisco, p. 297
Walker A.R., 1987, MNRAS, 229, 31
Whittet D.C.B., van Breda I.G., 1980, MNRAS, 192, 467
Yadav R.K.S., Sagar R., 2002, MNRAS, 337, 133

This paper has been typeset from a TEX/LATEX file prepared by the author.